

REPORT DOCUMENTATION PAGE

AFRL-SR-BL-TR-98-

0140

Public reporting burden for this collection of information is estimated to average 1 hour per response, including the time for reviewing instructions, searching existing data sources, gathering the required data, reviewing and completing the collection of information. Send comments regarding this burden estimate or any other aspect of this collection of information, including suggestions for reducing the burden, to Washington Headquarters Services, Directorate for Information Operations and Reports, 1215 Jefferson Davis Highway, Suite 1204, Arlington, VA 22202-4302, and to the Office of Management and Budget, Paperwork Reduction Project (1070-0187).

Reviewing
Information

1. AGENCY USE ONLY (Leave blank)		2. REPORT DATE 31 Oct 97		3. REPORT TYPE AND DATES COVERED FINAL TECH REPORT, 01 SEP 94 TO 31 AUG 97	
4. TITLE AND SUBTITLE Motion Planning for Energy Management in Autonomous Vehicles				5. FUNDING NUMBERS F49620-94-1-0414	
6. AUTHOR(S) Dr. John Baillieul					
7. PERFORMING ORGANIZATION NAME(S) AND ADDRESS(ES) Dept of Aerospace/Mechanical Engineering Boston University Boston MA 02215				8. PERFORMING ORGANIZATION REPORT NUMBER	
9. SPONSORING/MONITORING AGENCY NAME(S) AND ADDRESS(ES) AFOSR/NM 110 Duncan Avenue Suite B115 Bolling AFB DC 20332-8050				10. SPONSORING/MONITORING AGENCY REPORT NUMBER	
11. SUPPLEMENTARY NOTES					
12a. DISTRIBUTION AVAILABILITY STATEMENT Approved for public release; distribution unlimited.					
13. ABSTRACT (Maximum 200 words) This report provides a technical overview of research supported under an AASERT (Augmentation Awards for Science and Engineering Research Training) grant administered by the U.S. Air Force Office of Scientific Research. The grant was tied to a parent grant AFOSR-90-0226 and its follow-on F49620-96-1-0059, both of which bear the title "The Nonlinear Control Theory of Complex Mechanical Systems". The period of performance of the subject AASERT grant was Sep 94 through Aug 97. Funds from this grant were used to support the PhD thesis research of Geoffry Howell as stipulated in the original proposal submitted in the Fall of 1993. Mr. Howell is expected to finish his dissertation and all degree requirements this year. The research described in this report (and which will be reported in greater detail in Geoff Howell's dissertation) is concerned with two interrelated themes in the control of super-actuated (or underactuated) mechanical systems: (1) how to control the degrees of freedom which are directly actuated without eliciting undesired behavior in the unactuated degrees of freedom, and (2) how to prescribe motions of the directly actuated degrees of freedom to achieve motion objectives for the degrees of freedom which are not directly controlled.					
14. SUBJECT TERMS				15. NUMBER OF PAGES 28	
				16. PRICE CODE	
17. SECURITY CLASSIFICATION OF REPORT Unclassified	18. SECURITY CLASSIFICATION OF THIS PAGE Unclassified	19. SECURITY CLASSIFICATION OF ABSTRACT Unclassified	20. LIMITATION OF ABSTRACT UL		

19980210 062

AIR FORCE Grant No. F49620-94-1-0414

FINAL REPORT

10/31/97

ASSERT Grant Project Title

Motion Planning for Energy Management in Autonomous Vehicles

Principal Investigator

John Baillieul
Department of Aerospace/Mechanical Engineering
Boston University
Boston, MA 02215
(617) 353-9848
johnb@engs.bu.edu

ABSTRACT

This report provides a technical overview of research supported under an ASSERT (Augmentation Awards for Science and Engineering Research Training) grant administered by the U.S. Air Force Office of Scientific Research. The grant was tied to a parent grant AFOSR-90-0226 and its follow-on F49620-96-1-0059, both of which bear the title *The Nonlinear Control Theory of Complex Mechanical Systems*. The period of performance of the subject ASSERT grant was September, 1994, through August 31, 1997. Funds from this grant were used to support the PhD thesis research of Geoffrey Howell as stipulated in the original proposal submitted in the Fall of 1993. Mr. Howell is expected to finish his dissertation and all degree requirements in 1998. The research described in this report (and which will be reported in greater detail in Geoff Howell's dissertation) is concerned with two interrelated themes in the control of *super-articulated* (or underactuated) mechanical systems: (1) how to control the degrees of freedom which are directly actuated without eliciting undesired behavior in the unactuated degrees of freedom, and (2) how to prescribe motions of the directly actuated degrees of freedom to achieve motion objectives for the degrees of freedom which are not directly controlled.

Contents

1	Introduction and Report Summary	3
2	Control of Single Degree of Freedom Hamiltonian Systems with Impulsive Inputs	5
3	A Simple Actuated Walking Mechanism Controlled by the Dynamics of an Appended Mass	20

1 Introduction and Report Summary

The research discussed below has been aimed at a number of the mathematical and engineering problems arising in planning and controlling the motions of complex vehicles containing elastic, fluid, and other types of components which may store energy. This work is closely tied to a larger body of research of the P.I. (Baillieul) on the control theory of complex mechanical systems. Since the beginning of the ASSERT project, the scope of the work has been broadened somewhat to study the use of various energy-storing appendages to provide primary actuation in simple bipedal walking machines. The funds provided by the grant have supported the PhD studies of Geoffrey Howell. Mr. Howell's research has progressed to the point that the award of his (PhD) degree is expected in 1998. His thesis will document both theoretical and experimental work on motion planning and control of autonomous mobile mechanisms. Technical details of some of his work are reported here. The broader technical issues associated with our ongoing work on the control of mechanical systems have previously been reported in:

1. Final Report of AFOSR-90-0226 *The Nonlinear Control Theory of Complex Mechanical Systems* by J. Baillieul, submitted on April 29, 1996.
2. Annual Progress Report of F49620-96-1-0059 *The Nonlinear Control Theory of Complex Mechanical Systems* by J. Baillieul, submitted on October 15, 1997.

We refer to these reports for further details, and we note that the more recent of the two reports cites fifty one (51) archival publications which collectively document the research supported under both the ASSERT and parent grants.

The principal topics of the present report are:

1. Control of Single Degree of Freedom Hamiltonian Systems with Impulsive Inputs (Chapter 2 below), and
2. Analysis of the Pendulum-driven Rimless Wheel (Chapter 3 below).

An edited version of the paper appearing as Chapter 2 appeared in the *Proceedings of the 1996 IEEE Conference on Decision and Control*.

The unifying theme of the research herein described is the multiobjective control of mechanical systems. Howell's thesis will be concerned in part with controlled motions of simple

vehicles having dynamic loads (elastic bodies, fluid filled tanks, etc.) which can store energy. The objective in these control problems is to execute motions between prescribed points while managing the dynamics of the loads, which are not directly controlled and which respond to the motions of the vehicles. For instance, in moving a vehicle between prescribed points, we shall typically want the internal energy to be zero at the beginning and ending point. Other energy management objectives can also be considered.

The next two sections of the report treat some specific model systems in which we use directly controlled degrees of freedom to accomplish specified motion objectives for the degrees of freedom in the system which are not directly controlled. The swing-up and stabilization of a pendulum on a cart using impulsive inputs illustrates a novel approach to control which is relatively straightforward to implement (as reported) while at the same time being applicable to a wider class of nonlinear mechanical systems (work in progress). This research is part of a continuing effort to understand how the geometry of the wave form of an input, and in particular its frequency content, affects the dynamics of controlled nonlinear systems. Our goal is to understand how actuator inputs should be designed so as to be maximally effective in controlling the degrees of freedom which are not directly actuated in a super-articulated mechanism. Motivated by the signal characteristics seen in biological motor control, we have studied impulsive inputs to control multiple pendulum systems. While multiple pendula typically exhibit chaotic responses to smooth periodic forcing (e.g. by sinusoids), we have found that carefully designed impulse trains can be used to elicit a variety of interesting dynamic responses in such systems. The next chapter discusses this circle of ideas for a class of controlled single degree of freedom systems.

Another goal of our research on energy management in autonomous vehicles is to design biped robots where walking cycle is actuated by oscillatory motions of an attached pendulum. Completely passive biped robots have been constructed (by other researchers) which, given proper initial conditions, walk without intervention down slightly sloping ramps. The energy lost at each (totally inelastic) footfall is restored by the conversion of gravitational potential energy to kinetic energy. Our contribution to this line of research is to add a controlled pendulum-like appendage to the passive walker which may be "swung" in carefully designed patterns to cause the biped to walk on level surfaces and even up slight slopes. Preliminary analysis of such a mechanism appears in Chapter 3, below, and more complete results will appear in the forthcoming thesis of G.W. Howell.

Control of Single-Degree-of-Freedom Hamiltonian Systems with Impulsive Inputs

S. Weibel

Dept. of Aero/Mech Engineering
Boston University
Boston, MA 02215

G. Howell

Dept. of ECS Engineering
Boston University
Boston, MA 02215

J. Baillicul

Dept of Aero/Mech Engineering
Boston University
Boston, MA 02215

Abstract

In this paper, we develop a theory for the feedback control of single degree-of-freedom Hamiltonian systems, utilizing inputs which approximate δ -functions. The main idea is that by using "spikey" control inputs, it is possible to force the system to jump between energy levels. Since there is a correspondence between energy levels and orbits for Hamiltonian systems, this control of system energy results in control of the system dynamics. Impulsive control has proven useful in simulations and experiments involving the global reconfiguration of mechanical systems. We present application of the control to the cart and pendulum swing-up problem.

1 Introduction

Recent and planned real-time control implementations in our laboratory (See [7]) have led us to study the use of intermittent actuator pulses to control complex physical systems. While there are elements of modern digital control theory which are useful in developing pulse-modulated control designs, there are several interesting issues which are not fully addressed by existing theory. One general question, which we treat here in the special case of low-order Hamiltonian control systems, involves the timing of pulses. Motivated by results from biological motor control, ([5]), we find that the timing of actuator pulses can be effectively tailored to produce the maximally efficient transmission of energy through a complex multibody system. For the systems studied below, pulsed inputs are most effectively applied when the system passes near to certain "advantageous" points in the phase space. At these advantageous points, which lie along easily characterized curves in the phase plane, the system is maximally able to absorb energy from the pulse. Feedback of a non-classical type thus plays a role in our control theory of pulse modulated systems. While a general discussion of pulse-shaping and pulse-timing for motion control of legged robots, snake-like robots, and other mechanisms is beyond the scope of the present paper, we do provide very explicit results on optimal pulse timing for a broad class of low-order mechanical systems.

The paper is organized as follows. In Section 2, we describe the class of single degree-of-freedom (SDOF), velocity-controlled Hamiltonian systems which are the principal objects of study in the paper. The implementation of impulsive inputs is discussed, and a general formula for "optimal" application points in the phase space is given. (The objective is to apply an impulsive input to add or remove the maximum possible amount of total energy from the given degree of freedom.) Section 3 discusses control synthesis, taking into account the possibility of actuator saturation. Section 4

applies the method to the example of swing-up control of a pendulum on a cart. Both damped and undamped pendulum dynamics are considered, and the results here indicate that the idealized Hamiltonian models are useful in guiding the design of control laws for mechanical systems in which damping is present. We also describe an actual experimental implementation in which there is the added complexity of a fairly short track on which the cart is allowed to travel.

2 SDOF Hamiltonian Systems and Impulsive Inputs

2.1 Impulse Response of SDOF Hamiltonian Systems

Consider Hamiltonian systems of the form

$$H(p, q; U) = \frac{1}{2m} [p + mf(q)U(t)]^2 + V_a(q, U) \quad (1)$$

where $V_a(q, U)$ is the *augmented potential* [2]

$$V_a(q, U) = -\frac{1}{2}mU(t)^2 + V(q)$$

and where $U(t) = \int_0^t u(\tau)d\tau$, $f \in C^r(q)$, and $V_a \in C^r(q)$, $r \geq 2$. Systems of this type arise from a reduction procedure described in [2] for a class of velocity-controlled, single degree-of-freedom mechanical systems. The equations of motion corresponding to (1) are

$$\begin{aligned} \dot{q} &= \frac{1}{m} [p + mf(q)U(t)] \\ \dot{p} &= -[p + mf(q)U(t)] \frac{\partial f(q)}{\partial q} U(t) - \frac{\partial V_a(q)}{\partial q} \end{aligned} \quad (2)$$

We wish to use $u(t)$ to produce desired changes in (unforced, i.e. $U(t) \equiv u(t) \equiv 0$) system energy

$$H_0 = \frac{p^2}{2m} + V(q), \quad (3)$$

where we have introduced the shorthand notation $H_0(p, q) = H(p, q; 0)$. From (1) and (2), the instantaneous change in energy is

$$\frac{\partial H(p, q; U)}{\partial t} = [(p + mf(q)U(t)) f(q)] u(t) = F(p, q, U)u(t)$$

The change in energy on a time interval $t_0 \leq t \leq t_1$ is obtained by integrating $\partial H/\partial t$:

$$\Delta H(p, q; U) = \int_{t_0}^{t_1} F(p(t), q(t), U(t))u(t)dt \quad (4)$$

The goal of this paper is to show how to prescribe ΔH by appropriate choice of $u(\cdot)$. The emphasis will be on impulsive inputs, the most basic model for which is $u(t) = \delta(t - t')$ for $t_0 \leq t, t' \leq t_1$. With this choice, the corresponding $U(\cdot)$ in (4) is the Heaviside step function, and some care is involved in evaluating the product $u(t)U(t)$. (See, e.g., [9].) Since we concentrate on actual implementations in which impulses are well approximated by narrow square waves, it will be natural to adopt the (fairly standard) convention ([9]) that the product is given by $u(t)U(t) = \frac{1}{2}\delta(t - t')$. More specifically, suppose

$$u_w(t) = \begin{cases} 0 & \text{if } t < t' \\ \frac{1}{w} & \text{if } t' \leq t < t' + w \\ 0 & \text{if } t \geq t' + w \end{cases} \quad (5)$$

Then, we take

$$U_w(t) = \begin{cases} 0 & \text{if } t < t' \\ \frac{t-t'}{w} & \text{if } t' \leq t < t' + w \\ 1 & \text{if } t \geq t' + w \end{cases} \quad (6)$$

If $G(t)$ is any continuous function, and $t_0 < t' < t_1 - w$, then

$$\int_{t_0}^{t_1} G(t) u_w(t) U_w(t) dt = \frac{1}{w^2} \int_{t'}^{t'+w} G(t) (t - t') dt.$$

Elementary calculus (l'Hôpital's rule) shows that the limit as $w \rightarrow 0$ is $\frac{1}{2}G(t')$. Hence, the change in energy associated with the impulsive input $u(t) = k\delta(t - t')$ (where k is some "gain" coefficient) is

$$\Delta_\delta^k H(p, q) = kpf(q) + \frac{k^2}{2}mf(q)^2.$$

Using the square-wave approximation $u_w(t)$ for $\delta(t - t')$, we write

$$\Delta^k H_w(p, q) = \frac{1}{w} \int_{t'}^{t'+w} F(p(t), q(t), U_w(t)) dt. \quad (7)$$

We shall make use of the fact that $\lim_{w \rightarrow 0} \Delta^k H_w = \Delta_\delta^k H$, and more specifically we shall use the following theorem.

Theorem 1 *There exist numbers, $K > 0$ and $0 < \epsilon_0(p, q) \ll 1$ such that for $0 < \epsilon < \epsilon_0$,*

$$|(\Delta^k H_w|_{w=\epsilon}) - \Delta_\delta^k H| < K\epsilon$$

Proof: Without loss of generality, let $t' = 0$. We expand $\Delta^k H_w$ in a Taylor series around $\epsilon = 0$:

$$\int_0^\epsilon F(p, q, U_w) dt = \epsilon F(p_0, q_0, U_0) + \int_0^\epsilon \left[\left(\frac{\partial F}{\partial q} \dot{q} + \frac{\partial F}{\partial p} \dot{p} + \frac{\partial F}{\partial U} u \right) \right]_{t=0} t + \mathcal{O}(t^2) dt,$$

with $p_0 = p(0)$, $q_0 = q(0)$, and $U_0 = U(0)$. By (2) and $U(0) = 0$, we can show

$$\left\| \left(\frac{\partial F}{\partial q} \dot{q} + \frac{\partial F}{\partial p} \dot{p} + \frac{\partial F}{\partial U} u \right) \right\| < K,$$

where K is an $\mathcal{O}(1)$ constant. Therefore

$$\|\Delta^k H_w - \Delta_\delta^k H\| < \frac{1}{\epsilon} \int_0^\epsilon [Kt + \mathcal{O}(t^2)] dt < K\epsilon$$

which proves the theorem. \square

2.2 Maximal and Minimal Application Points

Suppose we have a system moving freely on an orbit of energy H_0 . Denote the set of points on this orbit $\Sigma_0 = \{(q_0, p_0) : H_0(q_0, p_0) = H_0\}$. For every point in Σ_0 , $\Delta_\delta H = \Delta_\delta^1 H$ defines a mapping $\Delta_\delta H : \Sigma_0 \times R \rightarrow R$, where we use the fact that q_0 and p_0 are related by H_0 . It is only natural to ask which points in Σ_0 maximize or minimize $\Delta_\delta H$. Extremal points $(p(q_{ext}), H_0, q_{ext})$ may be shown to satisfy the following equation:

$$f(q) \frac{\partial V_a}{\partial q} - 2m \frac{\partial f}{\partial q} (H_0 - V_a(q)) = \pm f(q) \frac{\partial f}{\partial q} \sqrt{2m(H_0 - V(q))}. \quad (8)$$

We define those points which minimize and maximize $|\Delta_\delta H|$ as follows.

Definition 1 A point $(p(q_{ext}, H_0), q_{ext}) \in \Sigma_0$ is called a maximal application point if q_{ext} maximizes $|\Delta_\delta H|_{\Sigma_0}|$. (These points may be found as solutions of equation (8).)

Definition 2 A point $(p(q, H_0), q) \in \Sigma_0$ is called a minimal application point if $\Delta_\delta H|_{\Sigma_0}(q) = 0$.

Remark 1 On some orbits Σ_0 , $\Delta_\delta H|_{\Sigma_0}(q)$ is never zero. (This happens, for instance, if Σ_0 consists of a single equilibrium point of the unforced dynamics.) Hence *minimal application points* defined in this way may not exist on some orbits.

As suggested by the presence of the absolute values in the preceding definitions, our interest is in the magnitude of the energy change produced by an impulse. We shall see in following sections that knowledge of the minimal and maximal application points is useful in control synthesis.

3 Control Synthesis for Planar Hamiltonian Systems

3.1 Shaping the Control Input

The theorem of §2 provides the basis for control synthesis with impulsive inputs. In control synthesis, our goal is to design a rectangular pulse which produces a desired change in energy. Suppose we choose our control input $u(t)$ to be

$$u(t) = kr(t) = \begin{cases} \frac{k}{w}, & t \in [t', t' + w) \\ 0, & t \notin [t', t' + w) \end{cases} \quad (9)$$

where k is a constant gain we will determine later, and $r(t)$ is a unit area rectangular pulse. Assuming w is sufficiently small, by Theorem 1,

$$\int_{t'}^{t'+w} F(p(t), q(t), U(t))r(t)dt = \Delta_\delta^k H(p(t'), q(t')) + \mathcal{O}(w),$$

where $\Delta_\delta^k H(p(t'), q(t')) = kp(t')f(q(t')) + \frac{k^2 m}{2}f(q(t'))^2$. Then given some desired energy state H_d , we choose k such that

$$H_d - H_0(p', q') = \Delta_\delta^k H(p(t'), q(t')) + \mathcal{O}(w). \quad (10)$$

where $(p', q') = (p(t'), q(t'))$. We compute the *ideal* gain k^I from the above equation: assuming $f(q(t')) \neq 0$, let k^I be the smaller of the two roots of the quadratic equation

$$H_d - H_0(p', q') = kp'f(q') + \frac{mk^2}{2}f(q')^2. \quad (11)$$

Remark 2 It is interesting that there are generally two roots to this “gain equation.” The physical reason, of course, is that our input should be thought of as a velocity, and this velocity may be applied in two different directions with different “levels of effort” to produce a desired ΔH . Note that it might happen that $H_d - H_0(p', q')$ is negative and of large magnitude such that there are no real gains k satisfying (11). We shall for the moment assume this does not happen, and we treat this case separately below.

If there are no modeling errors (i.e. if (1)-(2) describe the physical system exactly), then in the limit as $w \rightarrow 0$, the ideal gain k^I transfers the system from the initial energy state H_0 to a final energy state H_d in one step. In the non-ideal case in which pulses have finite non-zero width w , we shall show that under mild hypotheses a sequence of rectangular pulse inputs may be defined which steer the energy level toward H_d . A sufficient condition to be able to define such a sequence of pulses is that the zeros of $f(\cdot)$ are disjoint from the critical points of the potential function $V(\cdot)$ and do not accumulate at a critical point of $V(\cdot)$. Under this hypothesis, we show that the system cannot get stuck at a state (q', p') where $\Delta_\delta^k H = 0$. This is the essential content of the following theorem.

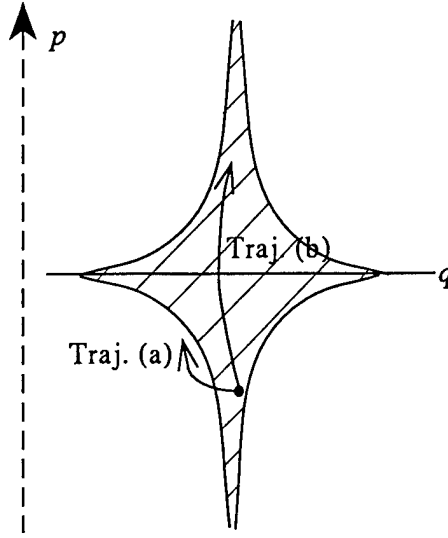


Figure 1: A component neighborhood of B_η

Theorem 2 Suppose there is given a Hamiltonian $H(p, q; U)$ as in (1) with corresponding equations of motion (2). We further suppose that $f(\cdot)$ and $V(\cdot)$ are analytic functions and that for some $\eta_0 > 0$

- (i) For $0 < \eta < \eta_0$, the set $\{q : f(q)^2 < \eta\}$ is composed of disjoint, open, finite intervals, each of length at most $\epsilon(\eta)$ where $\epsilon(\eta) = \mathcal{O}(\eta)$ as $\eta \rightarrow 0$, and
- (ii) $\{q : f(q)^2 \leq \eta_0\} \cap \{q : |\frac{\partial V}{\partial q}(q)| \leq \eta_0\} = \emptyset$.

Let H_0 be some initial energy state and H_d some desired final energy state. Let $w > 0$ be given such that $w \ll 1$. Consider a sequence of times $t_0 < t_1 < t_2 < \dots$ such that $(t_i - t_{i-1}) > w$, and define the sequence of rectangular pulses

$$u_i(t) = \begin{cases} \frac{k_i}{w} & t \in [t_{i-1}, t_{i-1} + w) \\ 0 & t \in [t_{i-1} + w, t_i) \end{cases} \quad (12)$$

where

$$k_i = \begin{cases} \text{smallest root } k \text{ of } H_d - H_{i-1} = kp'f(q') + \frac{mk^2}{2}f(q')^2 & \text{if } f(q')^2 > \eta_0 \\ 0 & \text{otherwise.} \end{cases}$$

(here $(p_{i-1}, q_{i-1}) = (p(t_{i-1}), q(t_{i-1}))$ and $H_{i-1} = H(p(t_{i-1}), q(t_{i-1}))$). Then the sequence $H_n = H_0(p_n, q_n) \rightarrow H_d$ as $n \rightarrow \infty$.

Proof Define for each $\eta > 0$

$$B_\eta = \{(q, p) : |pf(q)| + \frac{m}{2}f(q)^2 \leq \eta\}.$$

We claim that any unforced trajectory of (2) which enters or begins in B_{η_0} will leave B_{η_0} after a finite amount of time. Indeed, if $(q, p) \in B_{\eta_0}$, then $\frac{m}{2}f(q)^2 \leq \eta_0$, and under the hypothesis of the theorem, $|\frac{\partial V}{\partial q}(q)| > \eta_0$. Hence, $|\dot{p}| > \eta_0$, and we shall assume, without loss of generality, that $\dot{p} > \eta_0$. Under our hypothesis on $f(\cdot)$, the set B_{η_0} is the union of regions in the phase plane of the form depicted in Figure 1. Unforced trajectories of (2) evolve according to

$$\begin{pmatrix} \dot{q}(t) \\ \dot{p}(t) \end{pmatrix} = \begin{pmatrix} p \\ -\frac{\partial V}{\partial q}(q) \end{pmatrix},$$

and if $(q(t_0), p(t_0)) \in \mathcal{B}_{\eta_0}$, then either $(q(t), p(t))$ leaves \mathcal{B}_{η_0} (trajectory (a) in Figure 1) or $p(t)$ becomes positive (trajectory (b)). If $p(t)$ becomes positive, it must remain positive and bounded away from zero as long as $(q(t), p(t)) \in \mathcal{B}_{\eta_0}$. Hence $\dot{q}(t)$ will be positive and bounded away from zero, and as long as $(q(t), p(t)) \in \mathcal{B}_{\eta_0}$, $q(t)$ will continue to increase. Since $\{q : (q, p) \in \mathcal{B}_{\eta_0}\}$ is contained in the union of a set of subintervals of uniformly bounded width, $(q(t), p(t))$ must exit from \mathcal{B}_{η_0} after a finite amount of time. This proves that free (unforced) motions of (2) do not get stuck in regions of the phase plane where $f(q)^2 \leq \eta_0$. Thus, the definition of elements in the sequence of rectangular pulses prescribed in the statement of the theorem continues with the gains not “getting stuck” at zero until the system approaches the desired energy level.

Next we show that with impulse gains defined as in the statement of the theorem, the system moves through a sequence of energy levels H_n , such that $H_n \rightarrow H_d$ as n increases. The first energy transition is to

$$\begin{aligned} H_1 &= H_0 + \Delta^{k_1} H_w \\ &= H_0 + \Delta_\delta^{k_1} H + \mathcal{O}(w) \quad (\text{by Theorem 1}) \\ &= H_0 + H_d - H_0 + \mathcal{O}(w) \\ &= H_d + \mathcal{O}(w). \end{aligned}$$

In the limit as $w \rightarrow 0$, it would be possible to make the desired energy transition in a single step. For small $w > 0$, the system moves very nearly to the desired energy in the first step. After this, the result of the next rectangular pulse is a transition to the new energy level

$$H_2 = H_1 + \Delta^{k_2} H_w.$$

Rather than invoke Theorem 1 again at this point, we refine our estimate of $\Delta^{k_2} H_w$. One can show that for k_i defined as in the statement of the theorem that

$$\Delta^{k_i} H_w = \Delta_\delta^{k_i} H + M \cdot (H_d - H_{i-1}) \cdot w + o(k_i w), \quad (13)$$

where M is a constant which may be chosen to be independent of (q_{i-1}, p_{i-1}) . Since $H_d - H_1 = \mathcal{O}(w)$, we find

$$\begin{aligned} H_2 &= H_1 + \Delta_\delta^{k_2} H + M \cdot \mathcal{O}(w^2) + o(k_i w) \\ &= H_1 + H_d - H_1 + \mathcal{O}(w^2) \\ &= H_d + \mathcal{O}(w^2). \end{aligned}$$

Reapplying this type of analysis, it is possible to conclude that $H_d - H_n = \mathcal{O}(w^n)$, proving the theorem. \square

There are two important ways in which the rectangular pulses we take as our inputs must actually differ from δ -function idealizations. First, because time is quantized in our digital hardware, there is a minimum pulse-width which can be achieved. For the purposes of the present paper, we shall assume, however, that our pulse widths w may be chosen as small as needed. There are also magnitude constraints on the forces which our actuators may produce. Equation (9) does not account for possible limitations on the magnitude of k^I/w . It is possible that for some values of k^I , the input k^I/w may not be physically realizable by the source of actuation. In this case, a longer sequence of rectangular pulses $u_i(p, q, t)$ may be required to achieve a desired energy state.

To account for constraints on the output magnitude of the system’s actuator, we must make appropriate modifications to the control strategy of Theorem 2. Let the maximum allowable gain k be denoted k_{max} , and assume the restrictions on input gain are symmetric with respect to sign. Then, the control input $u(t)$ is adjusted to account for this maximum value:

$$u(t) = \begin{cases} \frac{1}{w} \text{sgn}(k^I) \cdot \min(\|k^I\|, k_{max}) & t \in [t', t' + w) \\ 0 & t \notin [t', t' + w) \end{cases}$$

We again control the system by prescribing a sequence of rectangular pulses applied at a sequence of times $t_0 < t_1 < \dots$. Under the hypotheses of Theorem 2, it is still possible to use magnitude-limited rectangular pulses to steer the system (2) between chosen energy levels. This is made precise in the next theorem.

Theorem 3 Suppose there is given a Hamiltonian $H(p, q; U)$ as in (1) with corresponding equations of motion (2). We further suppose that $f(\cdot)$ and $V(\cdot)$ are analytic functions and that for some $\eta_0 > 0$

(i) For $0 < \eta < \eta_0$, the set $\{q : f(q)^2 < \eta\}$ is composed of disjoint, open, finite intervals, each of length at most $\epsilon(\eta)$ where $\epsilon(\eta) = \mathcal{O}(\eta)$ as $\eta \rightarrow 0$, and

(ii) $\{q : f(q)^2 \leq \eta_0\} \cap \{q : |\frac{\partial V}{\partial q}(q)| \leq \eta_0\} = \emptyset$.

Let H_0 be some initial energy state and H_d some desired final energy state. Let $w > 0$ be given such that $w \ll 1$. Consider a sequence of times $t_0 < t_1 < t_2 < \dots$ such that $(t_i - t_{i-1}) > w$, and define the sequence of rectangular pulses

$$u_i(t) = \begin{cases} \frac{1}{w} \text{sgn}(k_i^I) \cdot \min(\|k_i^I\|, k_{max}) & t \in [t_{i-1}, t_{i-1} + w) \\ 0 & t \in [t_{i-1} + w, t_i) \end{cases} \quad (14)$$

where k_i^I is sequence of ideal gains defined in theorem 2. This sequence of rectangular pulse inputs steers the system (2) through a sequence of energy levels H_i such that as i increases $H_i \rightarrow H_d$.

Proof (Sketch.) Suppose pulse magnitudes are bounded by k_{max} . The change in energy produced by applying the rectangular pulse (of amplitude k and width w)

$$u(t) = \begin{cases} k & t \in [t', t' + w) \\ 0 & t \notin [t', t' + w) \end{cases}$$

to (2) is

$$\Delta^k H_w = kwpf(q) + k^2 w^2 \frac{m}{2} f(q)^2 + o(w).$$

Essentially the same argument that was applied to prove theorem 2 establishes the conclusion of the present theorem. Of course, convergence is slower by a factor of $\mathcal{O}(1/w)$. \square

Remark 3 The two theorems proved in this section show that very simple pulse modulated control designs may be applied under mild assumptions to steer a single degree of freedom Hamiltonian system of the form (2) between desired energy curves in the phase plane. By combining such pulse-modulated steering with the free evolution of the dynamics along constant energy curves, it is possible to steer the system between states which may be of interest. While this type of control has been shown to work even in the presence of constraining amplitude bounds on the inputs, it remains to show how effectively pulse modulated control may be applied in situations where speed and input energy are of concern. In the next section, we address the question of optimal timing of pulses.

4 Impulsive Control of the Cart and Pendulum

4.1 System Model

In this section, we consider the problem of controlling the cart and pendulum, as shown in Figure 2. In the figure, θ represents the angular displacement of the pendulum from vertical, and q_0 is the position of the cart. M and m are the masses of the cart and pendulum, respectively, ℓ is the length of the pendulum, and g is the gravitational acceleration. The system in Figure 2 has the Hamiltonian

$$H(p, q; U) = \frac{1}{2m\ell^2} [p - m\ell \cos q U(t)]^2 - \frac{1}{2} m U(t)^2 + mg\ell(1 - \cos q) \quad (15)$$

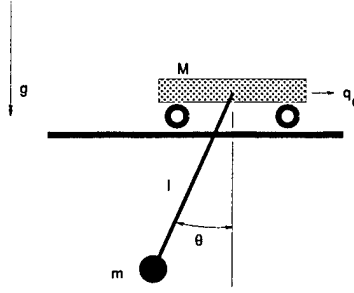


Figure 2: The Cart and Pendulum

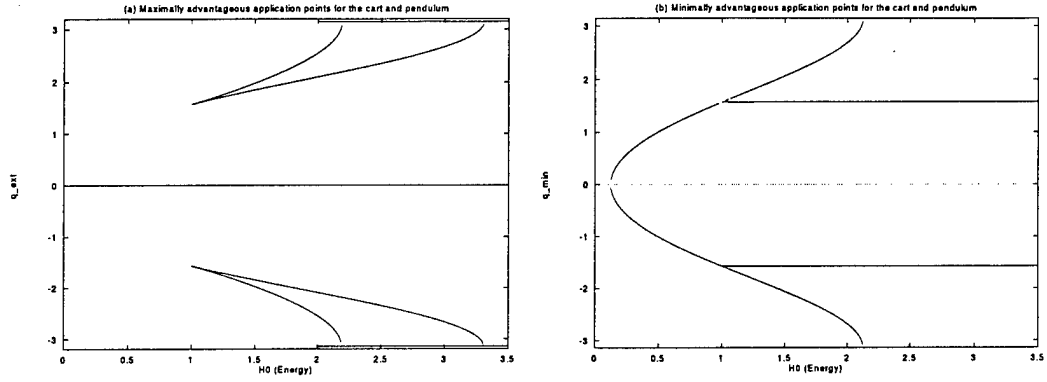


Figure 3: Maximal and minimal application points for the cart and pendulum, where $m = g = \ell = 1$. Note that a minimal application point does not exist for $H_0 < 0.13$.

where $q = \theta$ and corresponding equations of motion

$$\dot{q} = \frac{1}{m\ell^2} (p - m\ell \cos q U(t)) \quad (16)$$

$$\dot{p} = -\frac{1}{\ell} [p - m\ell \cos q U(t)] \sin q U(t) + mg\ell \sin q. \quad (17)$$

4.2 Effects of Input Shape on Change in Energy

From (15), we have

$$F(p, q, U) = -\left(\frac{1}{\ell}(p - m\ell \cos q U(t)) \cos q + mU(t)\right)$$

If $u(t) = \delta(t - t')$, then

$$\Delta_\delta H = -\frac{1}{\ell} (p(t') - m\ell \cos q(t')) \cos q(t')$$

From (8), the maximal application points are those points $(p, q) \in \Sigma_0$ which satisfy

$$-g \sin q \cos q - p^2 \sin q = p \sin q \cos q, \quad (18)$$

where $p = p(q, H_0) = \pm \sqrt{2(H_0 - (1 - \cos q))}$. The minimal application points are simply those points $(p, q) \in \Sigma_0$ for which $\Delta H_\delta \equiv 0$. Plots obtained numerically for the maximal and minimal application points are shown in Figures 3a,b, where m, g , and ℓ were all taken to be 1. Note in

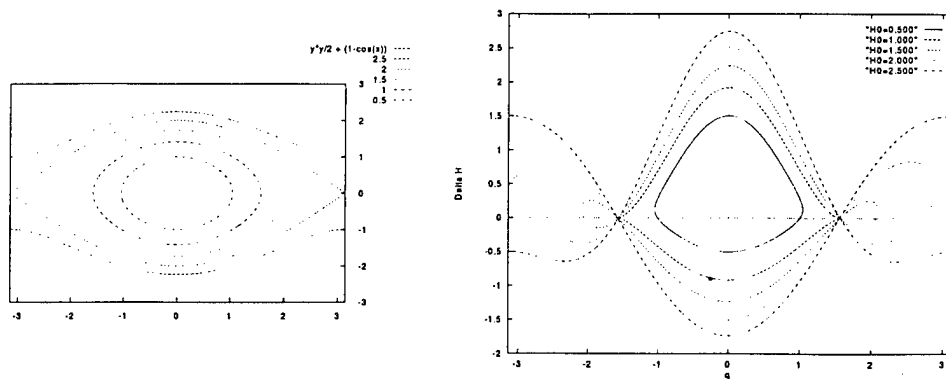


Figure 4: (a) Selected Constant Energy Curves and (b) Corresponding ΔH_w for the Cart and Pendulum

Figure 3b that a minimal application point does not exist for $H_0 < 0.13$. As shall be seen in the next figure, this is because the ΔH_δ curve lies entirely above the q -axis for energy levels smaller than 0.13. The number of solutions for each changes at the energy $H_0 = 1$, where the orbit Σ_0 passes through $(q, p) = (\pm\pi/2, 0)$. Nonlinear controllability analysis[10] reveals that the system is neither locally nor globally accessible at these states. In Figure 3a, two new branches of solutions are created, both of which terminate at $q = \pm\pi$ within the plotted range of H_0 . Another branch of solutions at $q = \pm\pi$ forms for $H_0 \geq 2$. The solution corresponding to $H_0 = 2$ is the separatrix solution, as shall be seen in the next set of figures. The two “bifurcated” branches of solutions in Figure 3a ultimately limit on the $q = \pm\pi$ solutions. In Figure 3b, a new branch $q = \pm\pi/2$ is created at $H_0 = 1$, and exists for all H_0 . Therefore, an input applied at $q = \pm\pi/2$ for $H_0 > 1$ produces no change in energy. The original branch of solutions in Figure 3b also limits at $q = \pm\pi$, but does not persist. Like $q = \pm\pi/2$ at $H_0 = 1$, the value of H_0 where $q = \pm\pi$ is both a maximal and minimal application point. These degeneracies are the result of the presence of cusps in ΔH_δ at the degenerate points.

Results of numerical investigations of ΔH_w for varying H_0 and w are shown in Figures 4 and 5. Figure 4a shows various orbits of the unforced, undamped pendulum for different energies H_0 . The images of the orbits in Figure 4a are shown in Figure 4b. The curves in Figure 4b were not determined by direct computation of $\Delta H_w(p_0, q_0)$. Rather, they were computed by running simulations of the pendulum system with a pulse applied at (p_0, q_0) , and then measuring the change in energy. In the simulations, parameter values $m = g = \ell = 1$ and $w = 0.01$ were used, with a time step of 0.001. These experimental curves closely match curves obtained from ΔH_δ , and confirm our earlier observations on maximal and minimal application points.

Figure 5 shows the effect of variations in w , given initial conditions with energy H_0 . Parameter values used in simulations are listed in the following table:

Pulse width w	0.01	0.1	0.5
Mass m	1	1	1
Gravity g	1	1	1
Initial energy H_0	1	1	1
Integration time step	0.001	0.01	0.05

The effect of increasing w is to shift the values q^{max} to the right above the q -axis, and to the left below. It is also clear that the shifts of $\Delta H_{0.01}$ and $\Delta H_{0.1}$ were accurately predicted by Theorem 1. Note that the curves for ΔH_w that lie above the x -axis are for negative values of p , and similarly

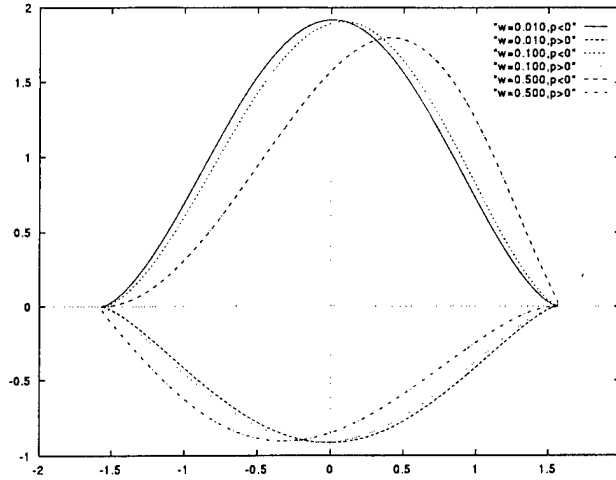


Figure 5: ΔH_w vs. q for the Cart and Pendulum, $H_0 = 1$

below the q -axis for positive p . The pulses used in these calculations were positive, meaning the input was a positive acceleration of the cart. We see that the pendulum experiences an increase in energy when the cart accelerates opposite the direction of the motion of the pendulum, and a decrease when the cart accelerates in the same direction. This may be interpreted as saying that the acceleration the pendulum feels is due to the change in relative velocities of the cart and pendulum. Also clear from the plot is a decrease in the maximum change in energy with increasing w , as evidenced in the plot of $\Delta H_{0.5}$.

4.3 Stabilization of the Inverted Equilibrium - Simulation Results

We now simulate the controlled stabilization of the inverted equilibrium of the pendulum. Because any lab experiment would require us to account for damping, we also consider impulsive control of the damped cart and pendulum under the assumption that damping is small. Given that our control synthesis is based on precise knowledge of the separatrix energies of the system, we would expect that impulsive control would fail in the presence of damping. We shall see that, in the absence of any compensation for damping, impulsive control does fail in the damped case. It performs well enough, however, that a hybrid control scheme can be developed which features the simplicity of impulsive control for swing-up and standard linear control for stabilization.

The results of the simulations are depicted in Figures 6 and 7. Parameter values used in the simulations are listed in the following table:

Parameter	Simulation 1	Simulation 2
Mass m	1	1
Gravity g	1	1
Damping coefficient c	0	0.05
Gain G_p	5	5
Initial p_0	0	0
Initial q_0	0	0
Desired energy H_d	2	2
Pulse width w	0.01	0.01
Duty cycle $(t_i - t_{i-1})$	0.25	0.25
Integration time step	0.001	0.001

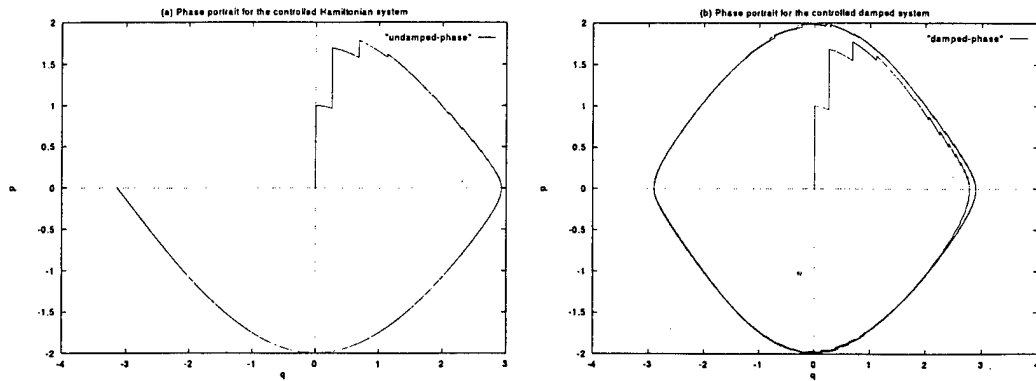


Figure 6: Phase Portraits for Undamped and Damped Systems with Impulsive Control

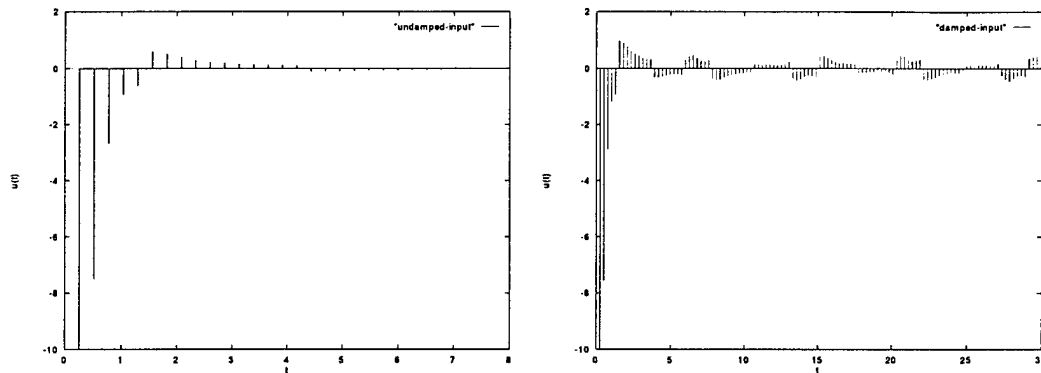


Figure 7: $u(t)$ vs. t for the Undamped and Damped Systems

Both the undamped and damped systems move near the desired energy within a small number of iterations (in this case, four), as predicted. The undamped system continues to move towards the separatrix, and stabilizes at $(-\pi, 0)$. The rapidity of convergence is seen in Figure 7, where input magnitude has fallen to less than 0.01 within three integration seconds. The damped system never converges to the desired energy. As seen in the figure, input magnitudes fall off quickly as the system approaches the separatrix, but oscillate about $u(t) = 0$ with small magnitude for the remainder of the simulation. However, the trajectory does pass close enough to the unstable fixed points to switch to linear control.

4.4 Stabilization of the Inverted Equilibrium - Experimental Results

Recent experiments in the Boston University Robotics Lab have verified that impulsive controls may be used in conjunction with linear control to regulate swing-up and stabilize the cart and pendulum experiment at the inverted equilibrium. A photograph of the experimental apparatus and a schematic of the system appear in Figure 8. The effective pendulum length, when it is modelled as a point mass pendulum, is 0.25 meters.

4.4.1 Control Synthesis

The control we choose for the pendulum swing-up maneuver involves applying impulses at the maximal application point of $q(t_i) = 0$ radians. The impulse application times t_i are determined as the experiment progresses. Each of these energy-pumping impulses increases the energy of both the

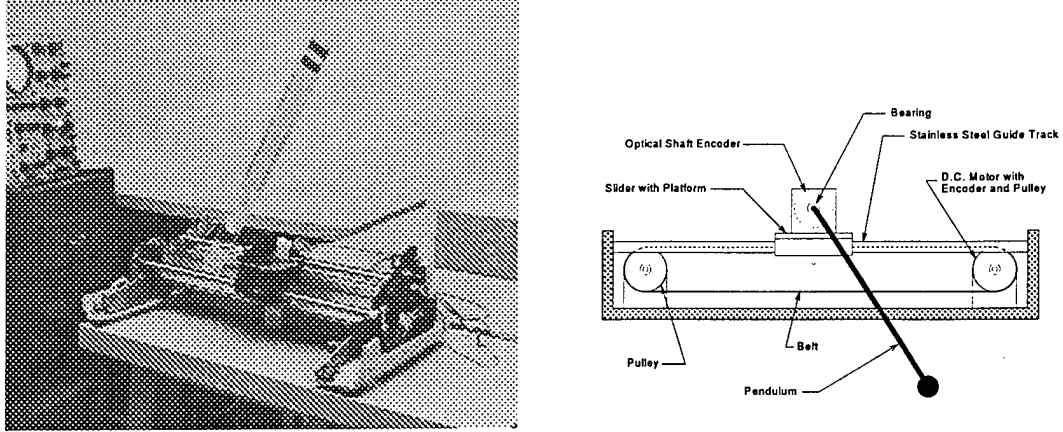


Figure 8: Cart with pendulum apparatus: (left) photograph and (right) schematic.

pendulum and the cart. The finite track length for the experimental apparatus shown in Figure 8, however, imposes restrictions on the shape of the control input. After each energy-pumping impulse, a counter-input must be applied to halt the cart before it crashes into its limit stop. To achieve the goal of inverting and balancing the pendulum, the counter-input must be designed such that it does not remove more energy from the pendulum than was provided by the energy-pumping impulse.

We choose for the counter-input a low-amplitude pulse of relatively long duration. The area of the counter-pulse is set to be equal to that of the energy-pumping impulse so that the counter-pulse will have an equal but opposite effect on the cart dynamics. The long duration of the counter-pulse ensures that the pendulum is farther away from the maximal application point during application than it was for the energy-pumping impulse. This causes it to have less of an effect on the pendulum energy. The net effect of each impulse/counter-pulse pair is to increase the pendulum energy.

After the impulsive input sequence has inverted the pendulum, a linear regulator is switched on to stabilize the system about its inverted position. The details for the design of such a regulator may be found in [8].

4.4.2 Experimental Results

The results of the control algorithm may be seen in the pendulum phase plot of Figure 9. The initial condition of the pendulum is $(q, \dot{q}) = (-0.30, 0.00)$. The pendulum velocity data is noisy because it was calculated from position encoder readings. Despite the noise, the increase in Hamiltonian energy due to the impulsive inputs may be seen as an increase in radius each time the angle of the pendulum crosses $q = 0$ radians.

The corresponding control input shown in Figure 10a is the acceleration of the cart. As noted in Theorem 1, square-wave approximations to the delta function have an upper bound on their duration, w . To focus the effect of the input near the maximal application point, the width of each impulse is set to be inversely proportional to the pendulum velocity, $\dot{q}(t_i)$. The impulses in Figure 10a may be seen getting taller and narrower as the experiment progresses. Immediately following each impulse in this graph may be seen the related low-amplitude counter-pulse.

Figure 10b, which displays the cart velocity, shows that the counter-pulses indeed have an opposite effect on the cart energy by driving the velocity back down to zero. The abrupt change in cart velocity at $t = 4.75$ seconds reflects the action of the linear control law as the pendulum enters the

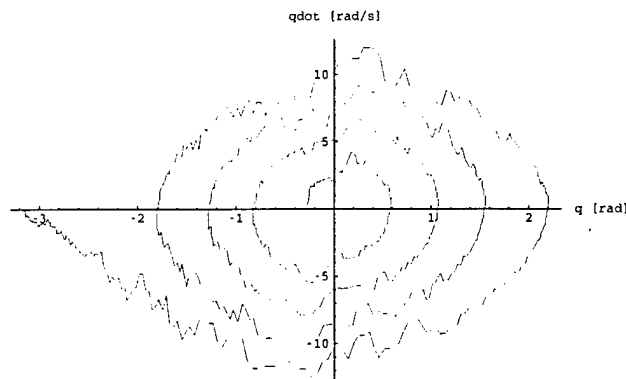


Figure 9: Pendulum phase plot showing effect of impulsive inputs and stabilization at the inverted equilibrium. Following the path of the pendulum in its clockwise spiral from the origin, an increase in radius (and hence, energy) is evident each time the pendulum received an impulsive input as it crossed $q = 0$ radians. A linear regulator stabilized the pendulum about its inverted equilibrium when the pendulum entered its region of stability at $(-\pi, 0)$.

region of stability of the linear regulator. Figure 10c shows the position of the cart as a function of time. Note that the entire swing-up maneuver required a total of less than 10 cm of cart track length.

Experimental results on controlling a swing-up maneuver and balancing the pendulum-on-a-cart system have so far been very encouraging. In preparing the full conference version of this paper, it is planned to provide comparisons with other approaches to swing-up and balancing control. (Cf. [4].) Short of this at the present time, we note two advantages of our impulsive control strategy: (i) The implementation required very few details about the physical characteristics of the pendulum-on-a-cart system; no effort to identify physical parameters was involved. (ii) As Theorem 2 indicates and experiments confirm, magnitude limits on the impulsive inputs have little effect on the system's ability to perform the swing-up.

5 Conclusion

This paper has presented preliminary results of a research program aimed at developing a theory of pulse-modulated control of mechanical systems. While our aim has been to develop a theory which can be applied to a wide class of mechanical systems (See [1]!), the emphasis here has been on velocity-controlled, single degree of freedom Hamiltonian systems. We have introduced an energy-based global control method for such systems based on inputs which approximate δ -functions. In §2, we characterized the response of Hamiltonian systems to impulsive inputs. Using the change of energy produced by a δ -function input as a start for our analysis, we derived an estimate of the change in energy produced by a narrow rectangular pulse. By viewing our "change in energy function" ΔH_w as an operator on orbits of the unforced system, we derived expressions defining those points on the orbit at which an impulsive input would produce the maximum and minimum changes in energy. This information was used in §3 as a basis for the synthesis of control laws. The proposed control law consists of a sequence of rectangular pulses which produce a desired net change in energy. Under some mild assumptions, we showed that a finite number of appropriately-sized inputs produces the desired finite change in energy. The theory of §2 and §3 was applied to the cart and pendulum in §4. In simulations and laboratory experiments, our simple control law performed

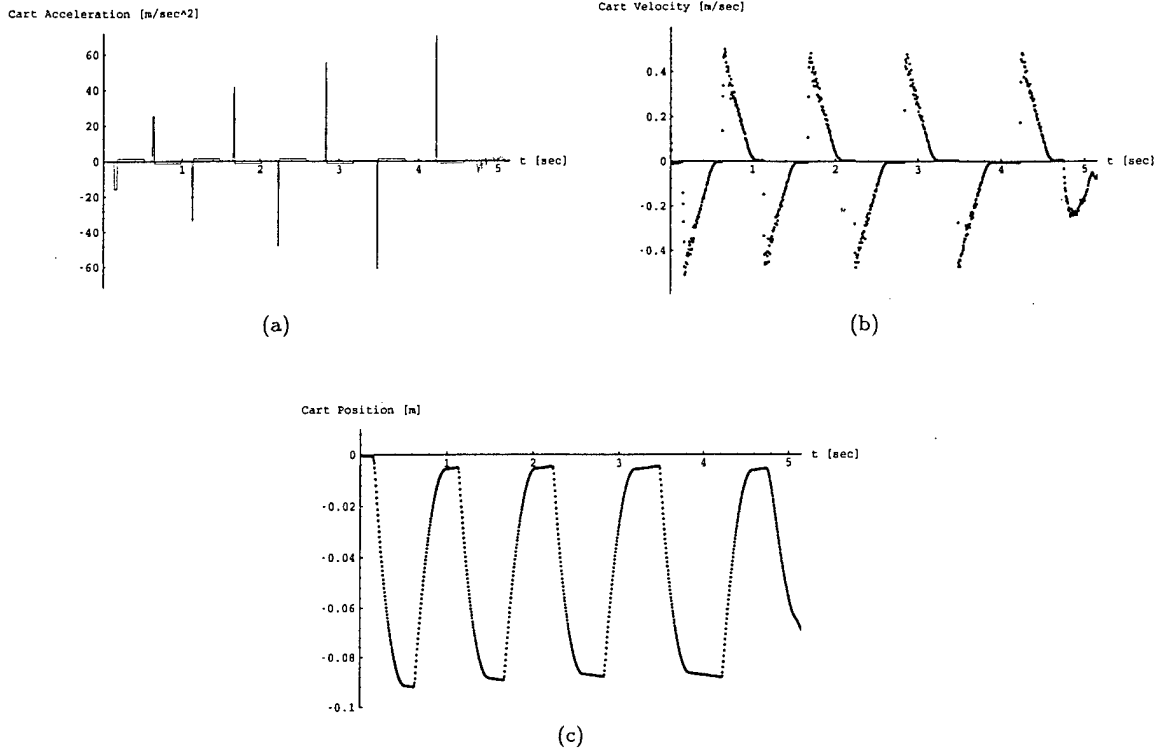


Figure 10: (a) Acceleration, (b) velocity, and (c) position of the cart vs. time for swing-up of pendulum.

pendulum swing-up, and in the simulations was able to steer the system to the stable manifold of the inverted equilibrium. In the experiments, impulsive control steered the system into a neighborhood of the inverted equilibrium, where a linear controller performed the final stabilization.

What makes this method of control attractive in these types of problems is its simplicity, which is best illustrated in the cart and pendulum application. In future publications, we will compare the performance of our swing-up controller to other control methods. One of our goals is to extend the analysis presented here to n -DOF Hamiltonian systems. Because of the nontrivial dynamics of multi-degree-of-freedom, coupled systems like kinematic chains, it is not completely clear how the theory presented here extends in the n -DOF case. We have found, however, that it is possible to extend the theory (with some modification) under certain conditions. This work has been shown to be useful in rigid body reorientation. We shall present this analysis in subsequent publications. Finally, current work has shown that impulsive controls can be used in conjunction with open-loop, "structure-creating" controls, such as high frequency periodic inputs (See [2],[3],[6], and [11].), to form closed-loop hybrid controllers. In this scenario, the impulsive control steers the system around the phase space structure created by the open-loop forcing. Details on this work will appear elsewhere.

References

- [1] D. Seto & J. Baillieul. Control problems in super-articulated mechanical systems. *IEEE Transactions on Automatic Control*, 39(12), December 1994.
- [2] J. Baillieul. Stable average motions of mechanical systems subject to periodic forcing. In *Dynamics and Control of Mechanical Systems: The Falling Cat and Related Problems: Fields Institute Communications*, Providence, R.I., 1993. American Mathematical Society.
- [3] J. Baillieul. Energy methods for stability of bilinear systems with oscillatory inputs. *Int'l J. of Robust and Nonlinear Control*, 5, July 1995.
- [4] M.W. Spong & D.J. Block. The pendubot: A mechatronic system for control research and education. In *The 34th Conf. on Decision and Control*, December 1995.
- [5] A.H. Goldstein, S. Rossignol, and S. Grillner. *Neural control of rhythmic movements in vertebrates*. Wiley series in neurobiology. Wiley, New York, 1988. A Wiley-Interscience publication.
- [6] J. Baillieul & B. Lehman. Open-loop control using oscillatory inputs. In *CRC Control Handbook*, W.S. Levine, Ed., Boca Raton, 1996.
- [7] D. Martin, S. Weibel, J. Baillieul, and D. Seto. Real-time control server. *Newsletter of the IEEE Robotics and Automation Society*, 5(2), March 1991.
- [8] S. Mori, H. Nishihara, and K. Furuta. Control of unstable mechanical system, control of pendulum. *Int. J. Control*, 23(5):673-692, 1976.
- [9] M. Oberguggenberger. *Multiplication of Distributions and Applications to Partial Differential Equations*. Longman Scientific & Technical Publishers (Wiley), London, 1992.
- [10] D. Seto. *Stabilization Problems in the Control of Super-Articulated Mechanical Systems*. PhD thesis, Boston University, 1992.
- [11] S. Weibel, J. Baillieul, and T.J. Kaper. Small amplitude periodic motions of rapidly forced mechanical systems. In *Proceedings of the 34th IEEE Conference on Decision and Control*, New Orleans, LA, 1995.

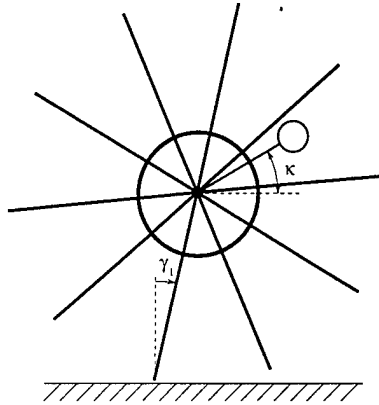


Figure 1: Pendulum-driven rimless wheel

ANALYSIS OF THE PENDULUM-DRIVEN RIMLESS WHEEL WITH CONSTANT PENDULUM ANGLE

G.W. Howell

Boston University
Robotics Laboratory
44 Cummington St.
Boston, MA 02215

January 14, 1998

Abstract – Tad McGeer had encouraging success in studying a rimless wheel rolling down a slope as a precursor to studying passive bipedal walking down a slope. In an effort to understand the method by which an otherwise passive walking robot might be controlled by a motorized pendulum mounted to its hip, we present here a study of a pendulum-driven rimless wheel, where a motor holds the pendulum at a constant angle with respect to world coordinates. This document describes the derivation of the system dynamics equation. Part of the dynamics is a momentum-conserving collision at each successive foot fall. This collision equation describes the transition of the system into the next step. Also described is a method of finding the steady-state trajectory through iterative simulation. Simulation data for a sample system is presented as an aid to the reader's tuition.

1 INTRODUCTION

The first task performed by Tad McGeer in developing his passive biped robot was to study the passive dynamics of a rimless wheel rolling down a slope [3]. From his study he found average wheel speeds for varying values of slope angle, wheel spoke separation, and wheel moment of inertia. This data helped him select physical parameters for his biped walker such that the leg swing period would match the speed of the walker. A similar procedure will allow us to design a pendulum-driven biped walker.

Figure 1 shows the pendulum-driven rimless wheel system. The rimless wheel is unactuated at the ground level and is free to rotate about the stance spoke without slipping. A motor connecting the pendulum to the wheel may, in general, force the pendulum to follow an arbitrarily specified trajectory. For this first analysis, however, the motor is used to maintain the pendulum at a constant angle, κ , with respect to the horizontal. Figure 1 shows the wheel rotating about the current stance spoke, during which time its behavior

is governed by the equation of motion (derived in section 2). At the instant the next spoke hits the ground, however, the impulsive collision will instantaneously change the speed of the wheel. To keep the pendulum at the constant angle κ , the motor must simultaneously apply an impulse to adjust the pendulum speed to match the new wheel speed. The collision equation is derived in section 3.

Section 4 describes the iterative simulation method of finding the steady state trajectory and features some simulation results for a sample rimless wheel system.

2 DYNAMICS EQUATIONS

The equations of motion for the pendulum-driven rimless wheel are generated by calculating the Lagrangian for the system, then taking the proper derivatives to form Lagrange's Equations. This section reports, briefly, on the details of finding the equations of motion.

Figure 2 shows the vectors and physical parameters needed to derive the equations of motion for the pendulum-driven wheel system. All spokes except for the stance spoke and the collision spoke have been

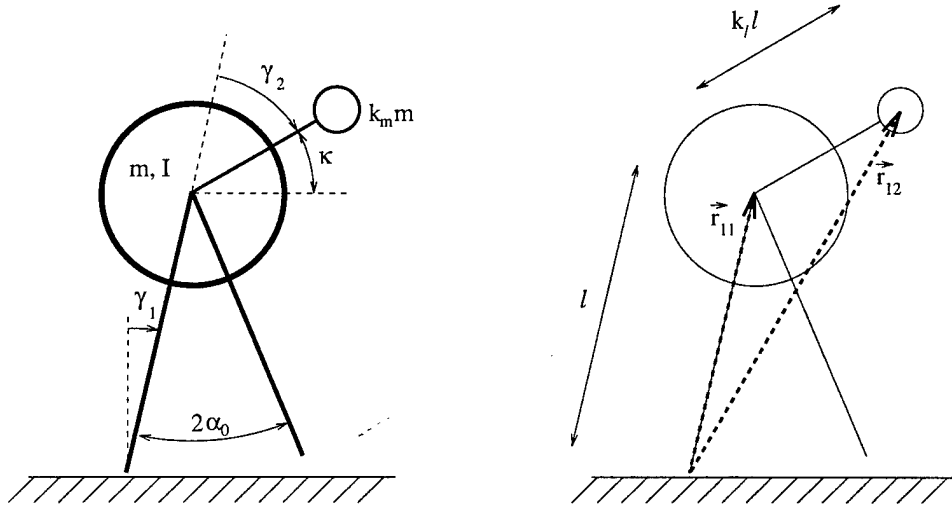


Figure 2: Parameters for the pendulum-driven wheel

omitted for clarity. The wheel has mass m and moment of inertia I . The angle between two consecutive spokes of the rimless wheel is $2\alpha_0$. The pendulum is a point mass with mass $k_m m$ at the end of a massless pendulum shaft of length $k_\ell \ell$. The vector \vec{r}_{11} points to the center of mass of the wheel with respect to the stance contact point. Similarly, the vector \vec{r}_{12} points to the tip mass of the pendulum bob with respect to the stance contact point. The vectors are given by

$$\begin{aligned}\vec{r}_{11} &= \ell \sin \gamma_1 \hat{i} + \ell \cos \gamma_1 \hat{k} \\ \vec{r}_{12} &= [\ell \sin \gamma_1 + k_\ell \ell \sin (\gamma_1 + \gamma_2)] \hat{i} + [\ell \cos \gamma_1 + k_\ell \ell \cos (\gamma_1 + \gamma_2)] \hat{k}\end{aligned}$$

The velocities of the wheel center of mass, \vec{v}_{11} , and the pendulum tip mass, \vec{v}_{12} , may be found by taking the time derivative of \vec{r}_{11} and \vec{r}_{12} , respectively.

The kinetic energy of the wheel is given by

$$T_{wheel} = \frac{1}{2} I \frac{d\gamma_1}{dt}^2 + \frac{1}{2} m \|\vec{v}_{11}\|^2.$$

For simplification purposes, we define the radius of gyration of the wheel, r_{gyr} , to satisfy the equation $I = m \ell^2 r_{gyr}^2$. Then the kinetic energy for the wheel becomes

$$T_{wheel} = \frac{1}{2} m \ell^2 r_{gyr}^2 \frac{d\gamma_1}{dt}^2 + \frac{1}{2} m \|\vec{v}_{11}\|^2. \quad (1)$$

The potential energy of the wheel is due to the force of gravity and is given by

$$V_{wheel} = mg r_{11_z}, \quad (2)$$

where r_{11_z} is the vertical component of the \vec{r}_{11} position vector. In the same fashion, the kinetic and potential energies of the pendulum may be found to be

$$\begin{aligned} T_{pend} &= \frac{1}{2} k_m m \|\vec{v}_{12}\|^2 \\ V_{pend} &= k_m mg r_{12_z} \end{aligned}$$

The Lagrangian, \mathcal{L} , for the system is given by the sum of all the kinetic energies minus the sum of all the potential energies:

$$\mathcal{L} = \sum T - \sum V$$

Since there is no form of actuation between the ground and the stance leg, while a motor with torque τ actuates the pendulum with respect to the wheel, Lagrange's equations for the system are

$$\frac{d}{dt} \frac{\partial \mathcal{L}}{\partial \left(\frac{d\gamma_1}{dt} \right)} - \frac{\partial \mathcal{L}}{\partial \gamma_1} = 0 \quad (3)$$

$$\frac{d}{dt} \frac{\partial \mathcal{L}}{\partial \left(\frac{d\gamma_2}{dt} \right)} - \frac{\partial \mathcal{L}}{\partial \gamma_2} = \tau \quad (4)$$

In this work, it is assumed that the motor is driven such that the pendulum maintains a constant angle, κ , with respect to the horizontal. From figure 2 we see that the relation between κ , γ_1 , and γ_2 is

$$\gamma_2 = \frac{\pi}{2} - \gamma_1 + \kappa.$$

For the pendulum to remain motionless, further, $\frac{d\gamma_2}{dt} = -\frac{d\gamma_1}{dt}$. Plugging these relations into the first equation of motion, equation 3, we find that the acceleration of the wheel is

$$\frac{d^2 \gamma_1}{dt^2} = \frac{k_m k_\ell \cos(\gamma_1 - \kappa) \frac{d\gamma_1}{dt}^2 + \frac{g}{l} (1 + k_m) \sin \gamma_1 - \frac{g}{l} k_m k_\ell \cos \kappa}{1 + k_m + r_{gyr}^2 - k_m k_\ell \sin(\gamma_1 - \kappa)} \quad (5)$$

To simplify the equations, a new time variable is introduced:

$$t_{new} = t \sqrt{\frac{g}{\ell}}$$

Letting "dots" denote differentiation with respect to t_{new} , equation 5 becomes

$$\ddot{\gamma}_1 = \frac{k_m k_\ell \cos(\gamma_1 - \kappa) \dot{\gamma}_1^2 + (1 + k_m) \sin \gamma_1 - k_m k_\ell \cos \kappa}{1 + k_m + r_{gyr}^2 - k_m k_\ell \sin(\gamma_1 - \kappa)} \quad (6)$$

Note that equation 6 is independent of the wheel mass, gravitational acceleration, and leg length. The manner in which the variables have been chosen requires that just five parameters be specified to completely define the pendulum-driven system: $(\alpha_0, r_{gyr}, k_m, k_\ell, \kappa)$.

3 COLLISION

When the next spoke of the rimless wheel collides with the ground, the system will instantaneously lose speed. The following analysis of the system collision follows one outlined by Hurmuzlu and Chang for planar kinematic chains [2]. It is based upon the laws of conservation of angular impulse and momentum,

conservation of linear impulse and momentum, an assumption on the elasticity of the collision, the frictional relationship between the horizontal and vertical components of the impulse delivered to the wheel by the ground, and the desired relationship between the final speeds of the wheel and the pendulum.

Figure 3 shows the three phases of the collision which must be considered. Figure 3a shows the wheel an instant before collision. The wheel is rotating about the left spoke with known speed $\dot{\gamma}_1$ while the pendulum is rotating about the hub with known speed $\dot{\gamma}_2$. The right spoke is shown as a dotted line to emphasize that it is not yet supporting the weight of the wheel. At the moment of impact, shown in figure 3b, the ground

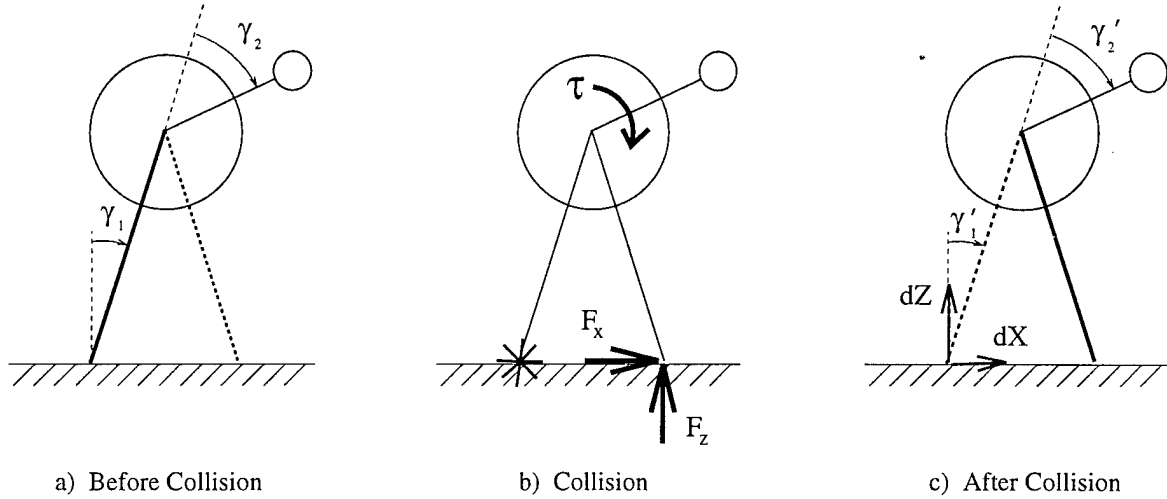


Figure 3: Parameters of interest during collision

under the collision foot applies an impulsive force with unknown components F_x and F_z . To maintain a desired relationship between the angular speeds of the wheel and pendulum, the motor applies an impulsive torque with unknown magnitude τ . For simplicity, let these impulsive forces be represented by Dirac delta functions: $\vec{F}(t) = \vec{F} \delta(t)$, $\tau(t) = \tau \delta(t)$. After the collision, figure 3c, the stance leg lifts off the ground with unknown speed components dX and dZ , while the wheel and pendulum have two new unknown rotational speeds, $\dot{\gamma}'_1$ and $\dot{\gamma}'_2$. The assumptions in this collision analysis are 1) the impact is instantaneous point impact, 2) the geometry of the system is unchanged during impact, and 3) all non-impulsive forces (due to gravity or centripetal acceleration) are small compared to the impulses and may be neglected. Note that all primed (') values in this analysis represent after-collision values.

We must solve for a vector with seven unknowns:

$$\vec{u} = (\dot{\gamma}'_1, \dot{\gamma}'_2, dX, dZ, F_x, F_z, \tau)^T$$

The only two known quantities we have are the speeds of the wheel and pendulum prior to impact: $\dot{\gamma} = (\dot{\gamma}_1, \dot{\gamma}_2)$. We may construct the matrix equation $A\vec{u} = B\dot{\gamma}$ with knowledge of the following conservation laws and relations.

Angular Impulse and Momentum – The principle of impulse and momentum states that the angular momentum of a system is only changed by the application of an external torque:

$$L + \sum \int_0^{t'} \tau_{ext} dt = L'. \quad (7)$$

In equation 7, L is the angular momentum of the system at time 0, τ_{ext} is a torque external to the system which is applied between times 0 and t' , and L' is the angular momentum of the system at time t' .

We have two separate angular momentum equations we may consider for the pendulum-driven rimless wheel. The first equation involves the angular momentum of the system about the stance contact point, L_s . [We could have chosen any arbitrary point to calculate the angular momentum about, but this choice of axis yields relatively simple results.] This angular momentum, before impact, is given as:

$$L_s = ml^2 r_{gr}^2 \dot{\gamma}_1 + m (\vec{r}_{11} \times \vec{v}_{11}) + k_m m (\vec{r}_{12} \times \vec{v}_{12})$$

At impact the torques from the impulsive forces and torque shown in figure 3b are added as provided by equation 7. Note that, as impulses, they require no further integration. The torque contribution from the ground forces is found by: Torque = $(\vec{r} \times \vec{F})$. The contribution from ground force \vec{F}_x is zero since the direction of this force vector goes through the axis of rotation. The motor torque impulse, $\vec{\tau}$, doesn't affect the angular momentum of the system because its torque is internal to the system. Hence the total external torque impulse felt by the system (about the stance point axis) is given by $(-2lF_z \sin \gamma_1)\delta(t)$. The conservation of angular momentum equation (7) becomes

$$L_s + \int (-2lF_z \sin \gamma_1)\delta(t)dt = L_s', \quad \text{which we write out explicitly as}$$

$$ml^2 r_{gyr}^2 \dot{\gamma}_1 + m (\vec{r}_{11} \times \vec{v}_{11}) + k_m m (\vec{r}_{12} \times \vec{v}_{12}) - 2lF_z \sin \gamma_1 = ml^2 r_{gyr}^2 \dot{\gamma}_1' + m (\vec{r}_{11} \times \vec{v}_{11}') + k_m m (\vec{r}_{12} \times \vec{v}_{12}') \quad (8)$$

where simple vector analysis shows that

$$\vec{v}_{11}' = \frac{d\vec{r}_{11}}{dt_{new}} + dX \hat{i} + dZ \hat{k},$$

$$\vec{v}_{12}' = \frac{d\vec{r}_{12}}{dt_{new}} + dX \hat{i} + dZ \hat{k},$$

and the rotational speeds in the \vec{v}' velocities are the ones after impact (i.e. $(\dot{\gamma}_1', \dot{\gamma}_2')$).

The second equation for the collision analysis involves the principle of angular impulse and momentum (equation 7) of just the pendulum about the wheel hub. The pendulum's angular momentum just before impact is:

$$L_p = k_m m ((\vec{r}_{12} - \vec{r}_{11}) \times \vec{v}_{12})$$

The only external torque contribution which the pendulum feels (since the ground forces act through a spoke and, hence, through the pendulum's axis of rotation) is the motor torque, τ . The conservation equation (7) thus becomes

$$L_p + \int \tau \delta(t)dt = L_p'$$

$$k_m m ((\vec{r}_{12} - \vec{r}_{11}) \times \vec{v}_{12}) + \tau = k_m m ((\vec{r}_{12} - \vec{r}_{11}) \times \vec{v}_{12}') \quad (9)$$

Linear Impulse and Momentum – The principle of linear impulse and momentum contributes two additional equations. The first equation obtained from this principle states that the total horizontal linear momentum of the system may only be modified by forces in the horizontal direction. Given that the linear momentum in the horizontal direction before and after collision is given by

$$P_{s_x} = m v_{11_x} + k_m m v_{12_x}, \quad \text{and}$$

$$P_{s_x}' = m v_{11_x}' + k_m m v_{12_x}',$$

the conservation of horizontal linear impulse and momentum equation is

$$P_{s_x} + \int F_x \delta(t)dt = P_{s_x}'$$

$$m v_{11_x} + k_m m v_{12_x} + F_x = m v_{11_x}' + k_m m v_{12_x}' \quad (10)$$

Similarly, another equation comes from consideration of the linear momentum of the system in the vertical direction:

$$P_{s_z} + \int F_z \delta(t)dt = P_{s_z}'$$

$$m v_{11_z} + k_m m v_{12_z} + F_z = m v_{11_z}' + k_m m v_{12_z}' \quad (11)$$

Coefficient of Restitution – The fifth system equation is the coefficient of restitution equation—a general collision equation. The coefficient of restitution is a representation of how much “bounce” there is in the system. In general, the restitution equation takes the form:

$$v_{B_z}' + e v_{B_z} = 0, \quad (12)$$

where v_{B_z} is the vertical velocity of the collision spoke w.r.t. an inertial frame. The assumption we will make for the rimless wheel is that the ground collisions are completely inelastic. Hence the coefficient of restitution, e , will be equal to zero and the restitution equation will become:

$$v_{B_z}' = 0$$

Resolving the Impulse Vector – The sixth system equation merely relates the two impulse vectors to each other by an unknown factor μ :

$$F_x = \mu F_y \quad (13)$$

This factor will relate to the coefficient of friction between the collision spoke and the ground.

Rotational Speed Requirements – The final system equation involves our desired speed relation between the pendulum and the wheel after collision:

$$\dot{\gamma}_2' = -\dot{\gamma}_1' \quad (14)$$

This keeps the pendulum at absolute angle κ even after the collision.

SOLUTION METHOD – Equations 8 through 14 may be combined into the single matrix equation $A\vec{u} = B\vec{\gamma}$ in the following form:

$$\begin{pmatrix} A_{11} & A_{12} & A_{13} & A_{14} & 0 & \frac{2 \sin \alpha_0}{m\ell} & 0 \\ A_{12} & -k_m k_\ell^2 & \frac{k_m k_\ell \sin \kappa}{\ell} & -\frac{k_m k_\ell \cos \kappa}{\ell} & 0 & 0 & \frac{1}{m\ell^2} \\ A_{13} & \frac{k_m k_\ell \sin \kappa}{\ell} & -\frac{1+k_m}{\ell^2} & 0 & \frac{1}{m\ell^2} & 0 & 0 \\ A_{14} & -\frac{k_m k_\ell \cos \kappa}{\ell} & 0 & -\frac{1+k_m}{\ell^2} & 0 & \frac{1}{m\ell^2} & 0 \\ \frac{2 \sin \alpha_0}{m\ell} & 0 & 0 & \frac{1}{m\ell^2} & 0 & \frac{1}{m\ell^2} & 0 \\ 0 & 0 & 0 & 0 & \frac{1}{m\ell^2} & -\frac{\mu}{m\ell^2} & 0 \\ \frac{1}{m\ell^2} & \frac{1}{m\ell^2} & 0 & 0 & 0 & 0 & 0 \end{pmatrix} \begin{pmatrix} \dot{\gamma}_1' \\ \dot{\gamma}_2' \\ dX \\ dZ \\ F_x \\ F_y \\ \tau \end{pmatrix} = \begin{pmatrix} A_{11} & A_{12} & A_{13} & A_{14} \\ A_{12} & -k_m k_\ell^2 & \frac{k_m k_\ell \sin \kappa}{\ell} & -\frac{k_m k_\ell \cos \kappa}{\ell} \\ A_{13} & \frac{k_m k_\ell \sin \kappa}{\ell} & -\frac{1+k_m}{\ell^2} & 0 \\ A_{14} & -\frac{k_m k_\ell \cos \kappa}{\ell} & 0 & -\frac{1+k_m}{\ell^2} \\ -\frac{2e \sin \alpha_0}{m\ell} & 0 & 0 & 0 \\ 0 & 0 & 0 & 0 \end{pmatrix} \begin{pmatrix} \dot{\gamma}_1 \\ \dot{\gamma}_2 \end{pmatrix} \quad (15)$$

where, for compactness of notation, we have labeled the following

$$\begin{aligned} A_{11} &= -1 - r_{gyr}^2 - k_m (1 + 2k_\ell \sin(\alpha_0 + \kappa) + k_\ell^2) \\ A_{12} &= -k_m k_\ell (k_\ell + \sin(\alpha_0 + \kappa)) \\ A_{13} &= \frac{(1 + k_m) \cos \alpha_0 + k_m k_\ell \sin \kappa}{\ell} \\ A_{14} &= -\frac{(1 + k_m) \sin \alpha_0 + k_m k_\ell \cos \kappa}{\ell} \end{aligned}$$

In solving equation 15 the first thing we do, as discussed before, is to set e to 0, which represents a perfectly inelastic collision. Then, since it is undesirable for the new stance spoke to slide after collision, dX is set to zero and equation 15 is solved for the unknown force coefficient which prevents slipping, μ :

$$\mu = \frac{-2 \cos \alpha_0 [(1 + k_m) \sin \alpha_0 - k_m k_\ell \cos \kappa]}{[(1 + k_m)(1 + \cos 2\alpha_0) + 2r_{gyr}^2 + 2k_m k_\ell \cos \alpha_0 \sin \kappa]} \quad (16)$$

Note that this force coefficient has the same relationship as one would expect of the friction relationship: $F_{friction} = \mu_{static} F_{normal}$. If $|\mu| < \mu_{static}$ for the surface then the friction force is sufficient and the wheel does not slip. After checking that the calculated μ is satisfactory, it is plugged back into equation 15 to solve for the remaining unknowns, including $\dot{\gamma}_1'$:

$$\frac{\dot{\gamma}_1'}{\dot{\gamma}_1} = \eta = \frac{(1 + k_m) \cos 2\alpha_0 + r_{gyr}^2 + k_m k_\ell \sin(\alpha_0 + \kappa)}{(1 + k_m) + r_{gyr}^2 - k_m k_\ell \sin(\alpha_0 - \kappa)} \quad (17)$$

Hence the speed of the pendulum-driven rimless wheel after collision is simply a function of the system parameters ($\alpha_0, r_{gyr}, k_m, k_\ell, \kappa$). The collision efficiency, η , indicates how much wheel speed remains after each collision. For example, if the wheel had a complete rim, rather than a finite number of individual spokes, α_0 would be zero and η would be one.

4 SIMULATION RESULTS

In this section, we define a default wheel with pendulum system. We describe the procedure used to find the steady-state trajectory. We analyze the collision equation for the default system to find the pendulum angle which yields the maximum collision efficiency. We present the results of a battery of system simulations which show the steady-state period versus pendulum angle.

One problem with simulating this system is the large number of system parameters which must be selected. There are five separate parameters which must be specified before the pendulum-driven rimless wheel system is defined: $(\alpha_0, r_{gyr}, k_m, k_l, \kappa)$. The temporary solution arrived at is to fix four of the parameters and call it the default system. Table 1 shows the parameters used for the default system. While the results from this default system will not be completely general, they are representative of a probable final system design.

Parameter	Value
α_0	0.314159
r_{gyr}	0.3
k_m	0.1
k_l	0.5

Table 1: Parameter values for default rimless wheel system.

Steady-state speed – A complete system simulation cycle starts with the stance spoke at $\gamma = \alpha_0$ and the wheel at some initial rotational velocity. The equation of motion, equation 6, is integrated until the stance spoke angle reaches α_0 , which indicates that the next spoke is ready to collide with the ground. At this point the after-collision velocity, $\dot{\gamma}'$, is calculated from equation 17. The simulation may be continued by restarting the system at $\gamma = \alpha_0$ with the new value of rotational velocity. The steady-state trajectory for the system may be found by iterating the simulation until the solution stabilizes.

Figure 4a shows the steady-state wheel trajectory of the default system with $\kappa = 0$ for two cycles of the motion. Figure 4b shows the corresponding velocity profile of the motion. At collision ($t_{new} = 2.277$) the wheel loses 15.3 % of its speed.

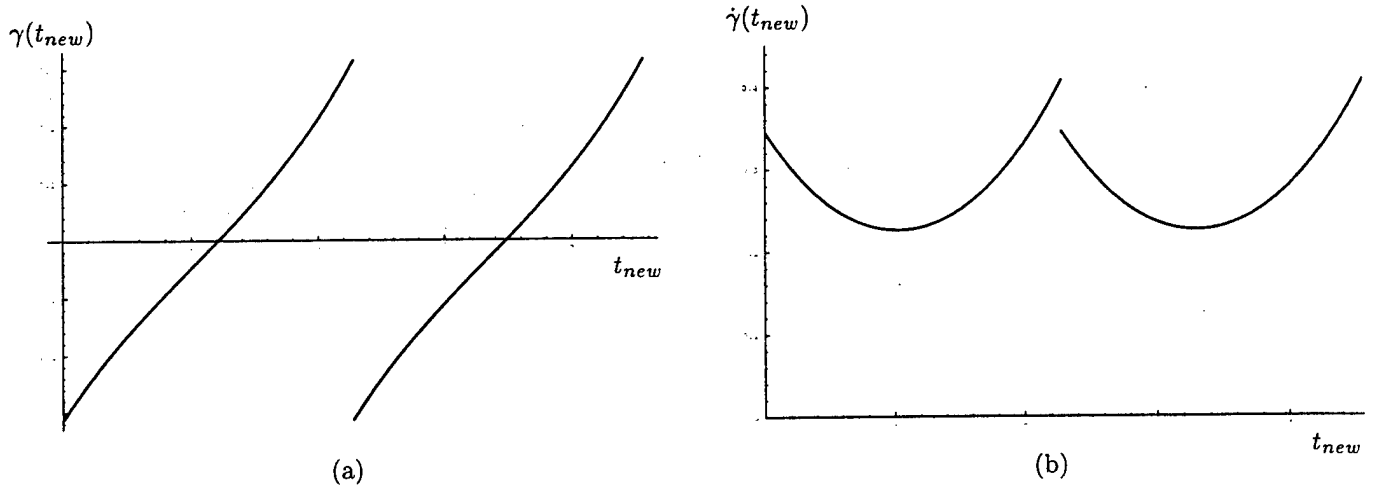


Figure 4: Steady-state trajectory of default system with $\kappa = 0$

One fruitful question we might ask regards the maximum collision efficiency, η , possible for the default system. The higher the collision efficiency, after all, the less energy is lost at each step. Figure 5 shows a plot of collision efficiency vs. pendulum angle for the default rimless wheel system. Differentiating equation 17 with respect to κ yields a maximum collision efficiency of 0.848 at $\kappa = 0.248$ rad.

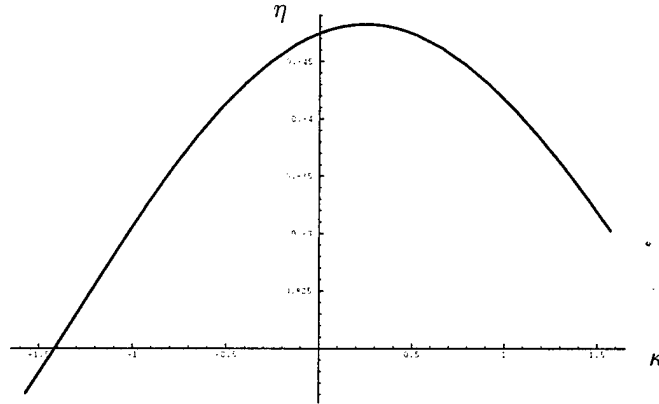


Figure 5: Plot of efficiency vs. pendulum angle for default system

Figure 6 shows simulation data for the steady-state period of the default system as a function of the pendulum angle, κ . Since the maximum efficiency was at $\kappa = 0.248$ rad, one might expect that the minimum

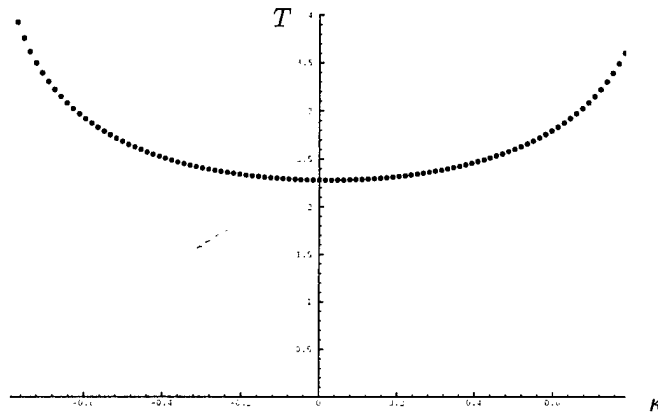


Figure 6: Plot of steady-state cycle period vs. pendulum angle for default system

cycle period (and hence the maximum steady-state wheel speed) in figure 6 would be located near $\kappa = 0.248$ rad. However, figure 6 shows that the maximum wheel speed occurs very close to $\kappa = 0$ rad, specifically at $\kappa = 0.02$ rad. This is because the acceleration of the wheel during the dynamics phase of the motion is maximized by $\kappa = 0$ rad. It is apparent that the pendulum's effect on the dynamics equation is more significant than its effect on the collision efficiency equation. Figure 7 shows the pendulum-driven rimless wheel system in the two competing configurations. In figure 7a, the pendulum angle maximizes the collision efficiency. Figure 7b shows the pendulum angle maximizing the steady-state speed of the wheel.

5 CONCLUSION

This paper described the pendulum-driven rimless wheel system. It derived the dynamics equation and the collision equation for such a system in the special case where the motor maintains the pendulum at a constant angle relative to horizontal. Simulation results were presented to show that the steady-state trajectory of such a system may be found by iterative simulation. The simulation results also showed that the maximum steady-state speed of the wheel will be arrived at when the pendulum is held out nearly horizontally.

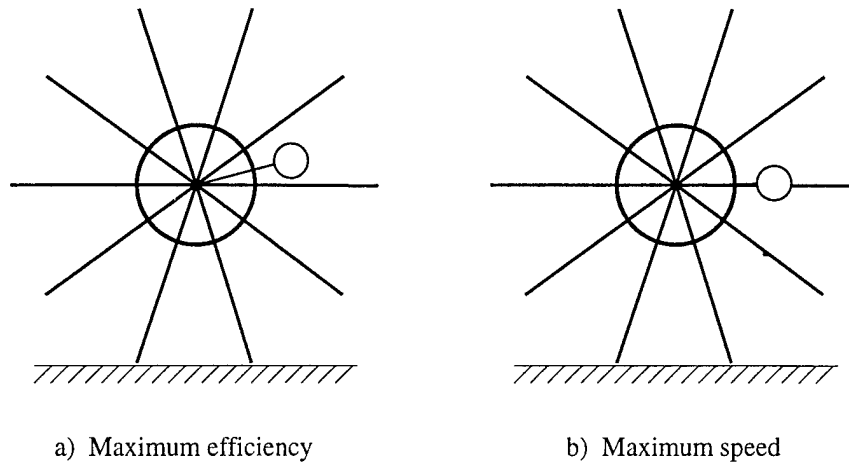


Figure 7: Pendulum configurations which maximize different values for the default system

REFERENCES

- [1] R. C. HIBBELER, *Engineering Mechanics. Statics and Dynamics*, Macmillan Publishing Company, New York, 1992. 6th Edition.
- [2] Y. HURMUZLU AND T. CHANG, *Rigid body collisions of a special class of planar kinematic chains*, IEEE Transactions on Systems, Man, and Cybernetics, 22 (1992), pp. 964-70.
- [3] T. MCGEER, *Passive dynamic walking*, International Journal of Robotics Research, 9 (1990), pp. 62-82.

Patented and is
distributed under the
terms of the
Creative Commons
Attribution-NonCommercial
4.0 International License

478 6000
WILDE
This is a
copy of the
document
numbered
478 6000
STINGO
Patented and is
distributed under the
terms of the
Creative Commons
Attribution-NonCommercial
4.0 International License